Journal of Vacuum Science and Technology A

RESEARCH ARTICLE | AUGUST 01 2024

Switching of kV-class Ga_2O_3 heterojunction vertical rectifiers

Special Collection: Commemorating the Career of Gerry Lucovsky

Jian-Sian Li ; Chao-Ching Chiang ; Hsiao-Hsuan Wan ; Meng-Hsun Yu; Yi-Ting Lin; Ying-Yu Yang; Fan Ren ; Yu-Te Liao ; Stephen J. Pearton

J. Vac. Sci. Technol. A 42, 053204 (2024)
https://doi.org/10.1116/6.0003839

JVST A
Journal of Vacuum Science & Technology A

ARTICLE

pubs.aip.org/avs/jva

Switching of kV-class Ga_2O_3 heterojunction vertical rectifiers

Cite as: J. Vac. Sci. Technol. A 42, 053204 (2024); doi: 10.1116/6.0003839
Submitted: 19 June 2024 · Accepted: 17 July 2024 ·
Published Online: 1 August 2024

Jian-Sian Li,[1] Chao-Ching Chiang,[1] Hsiao-Hsuan Wan,[1] Meng-Hsun Yu,[2] Yi-Ting Lin,[2] Ying-Yu Yang,[2] Fan Ren,[1] Yu-Te Liao,[2] and Stephen J. Pearton[3,a)]

AFFILIATIONS

[1]Department of Chemical Engineering, University of Florida, Gainesville, Florida 32611
[2]Department of Electronics and Electrical Engineering, National Yang Ming Chiao Tung University, Hsinchu 30010, Taiwan
[3]Department of Materials Science and Engineering, University of Florida, Gainesville, Florida 32611

Note: This paper is part of the Special Topic Collection Commemorating the Career of Gerry Lucovsky.
[a)]**Electronic mail:** spear@mse.ufl.edu

ABSTRACT

Switching of vertical 6.1 kV/4A NiO/Ga_2O_3 rectifiers from voltages up to 1.45 kV showed reverse recovery times of 75 ns, current slew rate of 39.0 A/μs, and energy loss of ~105 μW. These are the highest switching voltages reported for Ga_2O_3 rectifiers. To place the results in context, commercial 3.3 kV/5 A SiC merged PiN Schottky diodes showed reverse recovery times of 20 ns, current slew rate of 47.5 A/μs, and energy loss of ~67 μW. The validity of comparing unpackaged experimental Ga_2O_3 diodes with commercial Si or SiC diodes without considering their differences in chip size and consequently in capacitive charge and ON-resistance is restricted. However, the results show the rapid progress in these devices when compared to commercial SiC rectifiers.

I. INTRODUCTION

The electric vehicle (EV) market is undergoing rapid growth and is a significant factor propelling the market for SiC and GaN power devices.[1,2] These play a pivotal role in revolutionizing the future of EVs through three key mechanisms: (1) optimization of power electronics, (2) enhancement of vehicle efficiency and performance, and (3) facilitation of faster charging times. Compared to conventional Si, wide bandgap semiconductors have higher critical breakdown voltage and lower on-resistance.[1–9] These translate into reduced switching losses and the ability to withstand higher operating temperatures. Consequently, these materials and those with even larger bandgaps such as Ga_2O_3 achieve improved power conversion efficiency and superior overall system performance.[6–14] Additionally, their utilization contributes to the miniaturization, weight reduction, and cost optimization of electric vehicles. The extensive utilization of wide bandgap and ultrawide bandgap semiconductor devices in renewable energy systems (solar and wind) and EV charging infrastructure is anticipated to have a substantial positive impact on the environment during the ongoing transition toward electric mobility.[1–14]

The traction inverter converts the high-voltage direct current (DC) electrical energy stored in the battery pack into a regulated alternating current (AC) output within the EV propulsion system.[12–14] This AC output subsequently controls the torque and rotational speed of the electric motor. The efficiency of the power conversion process undertaken by the traction inverter directly influences the driving range achievable by the EV.[12–14] To optimize the cost-performance trade-off, some manufacturers are employing a hybrid switch architecture for traction inverters by using SiC MOSFETs in parallel with established trench-gate field-stop insulated-gate bipolar transistors (IGBTs).[15] This configuration aims to achieve a reduction in overall system costs without sacrificing the high-efficiency operation of SiC technology. This suggests other options such as use of Ga_2O_3 rectifiers in conjunction with Si, since the former is projected to be significantly less expensive than SiC.[16–25]

The basis of power electronic systems is the switch, which facilitates the conduction of high currents with minimal power losses in the on-state, while swiftly transitioning to high voltages in the off-state. When switching off a device in a forward operation, the stored charge will be swept out as the device enters a current

blocking state.[12–14] An ideal power rectifier would exhibit zero conduction and on-resistance in the on-state and withstand high voltage in the off-state without incurring power losses due to leakage current, real rectifiers deviate from this ideal.[12,13] All rectifiers, including Ga_2O_3 (Refs. 26–34), display a turn-on voltage and increased on-resistance during the on-state. In the off-state, they breakdown at a voltage dependent on critical field, doping, temperature, drift layer thickness and exhibit increased leakage current before breakdown.[35–48] During switching, the total power dissipation comprises two primary components: switching loss and conduction loss. The switching loss arises from leakage through the output capacitance, while the conduction loss is attributed to ohmic Joule heating through the on-state resistance.[11,12,40]

Calculations of total loss in wide- and ultrawide-bandgap semiconductors as a function of the device area with suggested operating conditions of 6.5 kV breakdown voltage, 6 kV reverse voltage, and 10 A forward current indicate that β-Ga_2O_3 potentially offers a higher efficiency and power density compared to SiC because of its low donor ionization energy and low impact ionization coefficients, attributed to low electron mobility, leading to high breakdown voltages.[37] Gong *et al.*[48] demonstrated the use of an optimized edge termination design based on NiO junction termination extension and $BaTiO_3$ field plate to achieve a robust avalanche performance in a NiO/Ga_2O_3 p-n heterojunction diode. The optimized design produced avalanche voltage and current of 2135 V/83 A, with avalanche energy density of 11.3 J/cm^2, comparable to SiC and GaN homojunctions. The devices exhibited no degradation after enduring 10 000 cycles of 2.1 kV/83 A avalanche stress.[48]

In this paper, we report the highest switching voltages to date for vertical geometry NiO/Ga_2O_3 rectifiers. The reverse recovery times and energy losses are compared with commercial kV-class SiC rectifiers. These devices are attractive options for power electronic converters.

II. EXPERIMENT

Figure 1 shows a schematic of the NiO/Ga_2O_3 heterojunction rectifier structure used in these experiments. The drift layer had thicknesses of ∼15 μm, with low n-type doping (∼9×10^{15} cm^{-3}). These were grown by halide vapor phase epitaxy on heavily doped n-type substrates [Sn-doped, (001), 10^{19} cm^{-3}] produced via edge-defined film-fed growth. Full-area backside Ohmic contacts were formed by e-beam evaporation of a Ti/Au stack, followed by annealing at 550 °C for 3 min. Ni/Au was used as the contact metal stack deposited via e-beam evaporation, with NiO bilayers deposited by low-power sputtering.[24,27,28] The doping concentrations for the NiO bilayer were 2.6×10^{18} cm^{-3} for the top 10 nm layer and 10^{18} cm^{-3} for the bottom 10 nm layer. Field plates, consisting of a bilayer SiN_X/SiO_2 dielectric extending 28 μm beyond the Ni/Au contact, were deposited using plasma-enhanced chemical vapor deposition. The extension of the NiO beyond the metal contact acts as a guard ring for additional edge termination.[24,27,28]

For comparison, packaged 3.3 kV, 5 A SiC merged PiN Schottky diodes were purchased from Gene SiC Semiconductor (GB05MPS22-263). The diode forward current was 5 A at ∼3 V forward bias. The packages were TO-263-7 model.

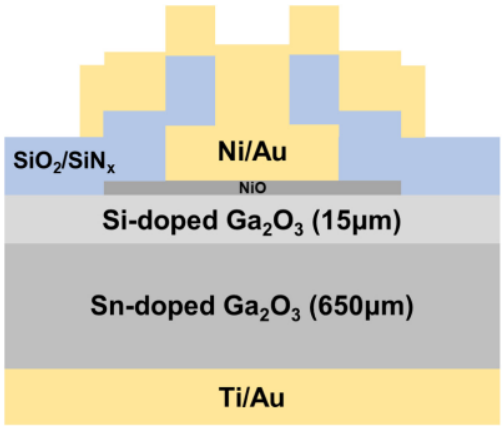

FIG. 1. Schematic of a vertical NiO/Ga_2O_3 rectifier.

The current–voltage (I–V) characteristics were measured under Fluorinert atmospheres at 25 °C using a Tektronix 371-B curve tracer and a Glassman high-voltage power supply. An Agilent 4156C parameter analyzer was employed for low voltage forward and reverse current characteristics. The reverse breakdown voltage was determined by the conventional criterion, defined as the reverse current reaching 0.1 A/cm^2. A mega-ohm resistor was used, and the voltage drop across the resistor was subtracted.[27,28]

The contact was verified by performing a forward sweep up to 5 V and a reverse sweep up to −100 V and confirming the I–V characteristics. The on-resistance (R_ON) was calculated from the derivative of voltage with respect to current (dV/dI) derived from the I–V characteristics. Corrections were made to account for the resistance contributed by external circuit components, including cables, chuck, and probe, which collectively amounted to 10 Ω.[27,28] This resistance was determined by measuring I–V while the cables, chuck, and probe were connected. Typical diode resistances were approximately 100 Ω at 5 V, which is ten times the external resistance. The calculated on-resistance values assumed a current spreading length of 10 μm, with a spreading angle of 45°. The on-resistance typically corresponds to unipolar drift resistance, which is generally lower than diffusion resistance. The I–V characteristics exhibited high reproducibility over areas measuring 1 cm^2 on the wafer, with absolute current variations of less than 20% at a given voltage.

To assess the diode's recovery time, a clamped inductive load test circuit was used for switching measurements.[39,40,49] This is shown schematically in Fig. 2 and its design and operation have been described in detail previously.[39,40,49] To measure the reverse recovery time of the rectifiers, τrr, defined as the time that taken for rectifiers recover to the current level of 25% of the reverse recovery current, Irr.

III. RESULTS AND DISCUSSION

Figure 3 shows the forward I–V and associated R_{ON} from the heterojunction NiO/Ga_2O_3 rectifier, as well as from the SiC

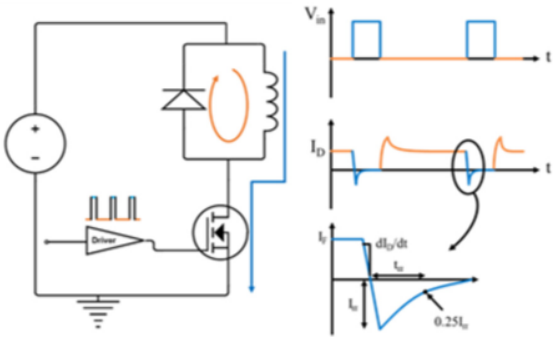

FIG. 2. Schematic of a clamped inductive load switching circuit and voltage/current waveforms of the circuit operations.

rectifier. Both reach a forward current of ~4 A at 5 V bias and have on-resistance of the order of 10 mΩ cm^2.

The reverse *J*–*V* characteristics are shown in Fig. 4(a). The breakdown voltage of the Ga_2O_3 device is 6.1 kV, while the SiC device is rated at 3.5 kV. We did not push those devices closer to breakdown due to a limited number of devices available. At low biases (<100 V), the reverse current density of the Ga_2O_3 rectifier is lower due to the larger bandgap, as shown in Fig. 4(b).

The on-off ratio when switching the devices from 3 V forward to the bias shown on the *x* axis is shown in Fig. 5. These values are all >10^{10} across the voltage range for both types of devices.

During the rectifier switching process (illustrated at the top of Fig. 2), a double pulse was utilized to drive the SiC transistor (GeneSiC G2R1000MT17D, a 1.7 kV, 3 A n-channel MOSFET). The duty cycle duration was adjusted to modulate the forward current of the Ga_2O_3 Schottky diode. The inductor (J. W. Miller 1140-153K-RC, 15 mH) was initially charged from a DC power

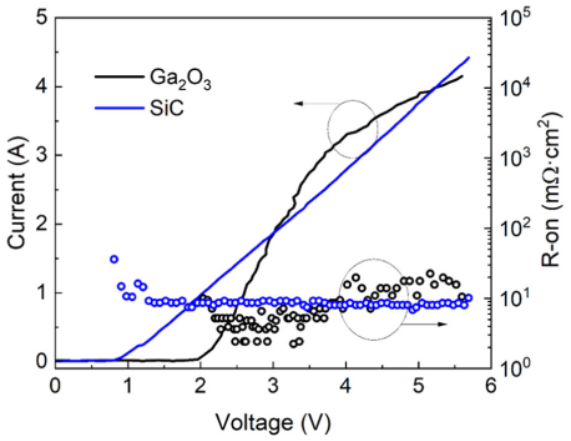

FIG. 3. Forward I–V characteristics and R_{ON} values from heterojunction NiO/Ga_2O_3 rectifiers and commercial SiC rectifiers.

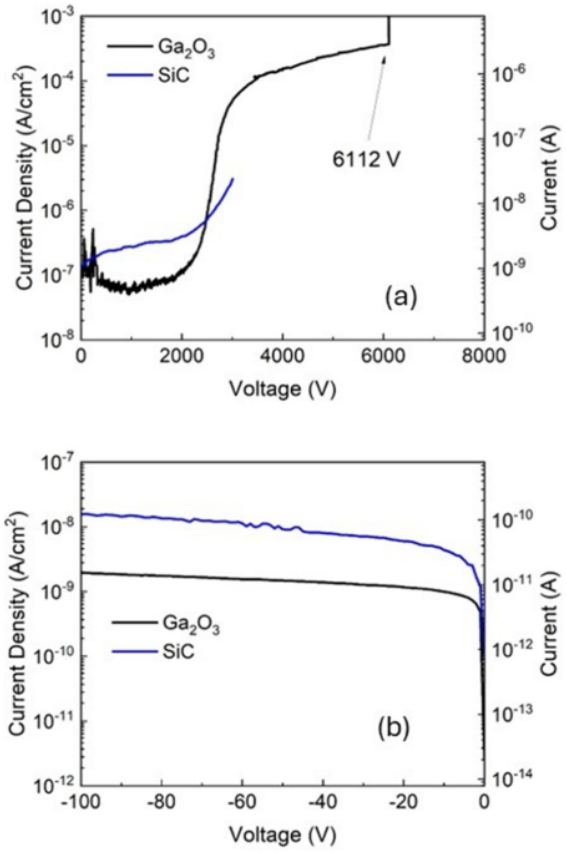

FIG. 4. Reverse J–V characteristics from heterojunction NiO/Ga_2O_3 rectifiers and commercial SiC rectifiers at (a) high voltage and (b) low voltage.

supply by activating the transistor. When the transistor was subsequently deactivated, the precharged inductor discharged through the forward-biased diode. Reactivating the transistor switched the rectifier from its on-state to its off-state, resulting in charge depletion. When evaluating unpackaged devices, it is important to consider that the high parasitic resistance of the measurement system results in recovery times being constrained by the silicon carbide (SiC) MOSFET within the switching circuit.[11,12] The accuracy of the switching measurements is further limited by the resistances of the probes and cables, as well as an additional resistor present on the circuit board. Consequently, while it is possible to correct for the on-resistance, the switch measurement results remain affected by these parasitic factors. Despite this limitation, these measurements still provide valuable qualitative comparisons. The combined parasitic resistance of the probe, probe station, and cables is quantified at 0.75 Ω.

Figure 6(a) shows the Ga_2O_3 rectifier switching waveforms when switching from either 1150 or 1450 V at duty cycles of 2% or 1%, respectively. The reverse recovery time from the 1150 V switching is 75 ns for a reverse recovery current of 0.68 A, while the

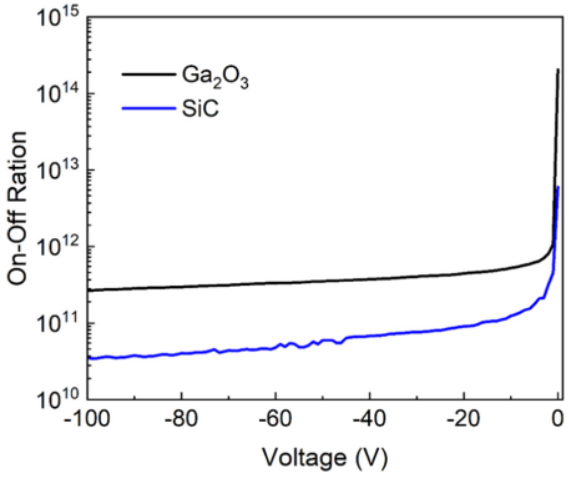

FIG. 5. On/off ratio from heterojunction NiO/Ga_2O_3 rectifiers and commercial SiC rectifiers when switching from 3 V forward to the reverse voltage shown on the *x* axis.

corresponding numbers are 74 ns and 0.88 A for 1450 V switching. The current slew rates were 52.2 and 39 A/μs, respectively, as summarized in Table I. The energy switching loss is defined as energy loss $= \int (I \times V)dt$ during the off-state period. The energy loss as a function of time during switching is shown in Fig. 6(b), with total energy loss of 77.6 μJ for switching from 1150 V and 104.5 μJ for switching from 1450 V.

The comparable results for SiC switching are shown in Figs. 7(a) and 7(b). In these cases, the switching from either 750 or 1300 V at duty cycles of 2% or 1%, respectively. The reverse recovery time from the 750 V switching is 20 ns for a reverse recovery current of 0.61 A, while the corresponding numbers are 20 ns and 0.55 A for 1300 V switching. The current slew rates were 61.4 and 47.5 A/μs, respectively, as also summarized in Table I. The energy loss as a function of time during the switching is shown in Fig. 7(b), with total energy loss of 61.9 μJ for switching from 750 V and 67.1 μJ for switching from 1300 V.

Breakdown in the rectifiers was found to occur at the edge of the anode contact. This is seen in the optical images of Fig. 8. When we purposely drove the devices to failure at the highest achievable switching voltages, pits were observed in the high field regions at the edges of the contact regions, i.e., the edge of the NiO extension.

How do we place our results in context? Figure 9 shows a compilation of reported results for reverse voltage versus forward current for vertical Ga_2O_3 rectifiers in the literature. The data in this current paper represent the highest reported switching voltages for Ga_2O_3 rectifiers. Figure 9 demonstrates the trade-off between a higher V_{ON} and the achievement of high V_B by presenting data from the literature on β-Ga_2O_3 rectifiers. For comparative purposes, typical values of commercial silicon (Si) p-n fast-recovery diodes and 4H-SiC junction barrier Schottky diodes

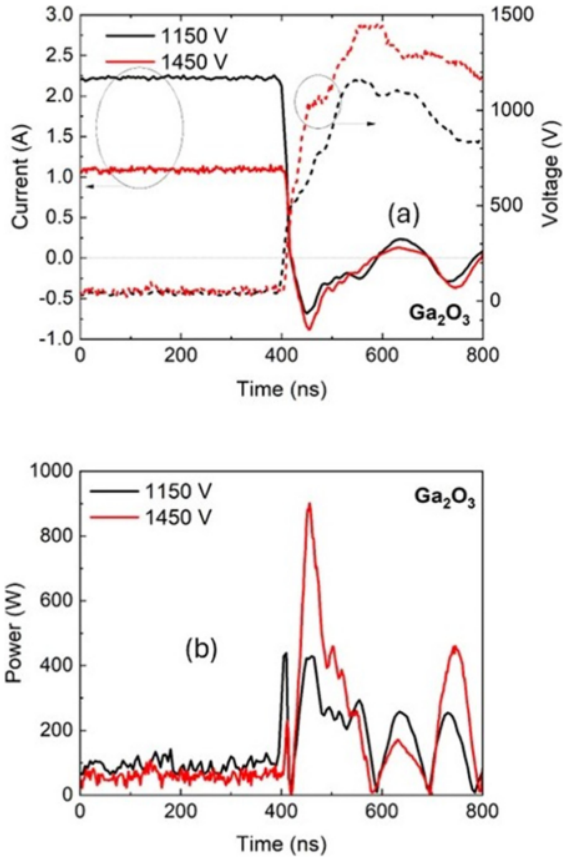

FIG. 6. Current (a) and power dissipation (b) switching waveforms for heterojunction NiO/Ga_2O_3 rectifiers when switching from either 1150 or 1450 V.

are also included.[37,50] A hypothetical boundary has been drawn to illustrate the experimental trade-off between V_{ON} and V_B based on the reported results. Wilhelmi *et al.*[12] evaluated 600 V β-Ga_2O_3 Schottky diodes as freewheeling diodes in a 400–200 V buck converter with output power up to 2 kW and switching frequencies up to 350 kHz. Double pulse tests were conducted at

TABLE I. Summary of switching parameters for experimental Ga_2O_3 and commercial SiC diodes.

	Reverse voltage (V)	Duty cycle (%)	T_{rr} (ns)	I_{rr} (A)	dI/dT (A/μs)	I_F (A)	Energy loss (μW)
Ga_2O_3	950	2	75	0.68	52.2	2.3	77.6
	1200	1	74	0.88	39	1.1	104.5
SiC	750	2	20	0.61	61.4	4.5	61.9
	1200	1	20	0.55	47.5	3.2	67.1

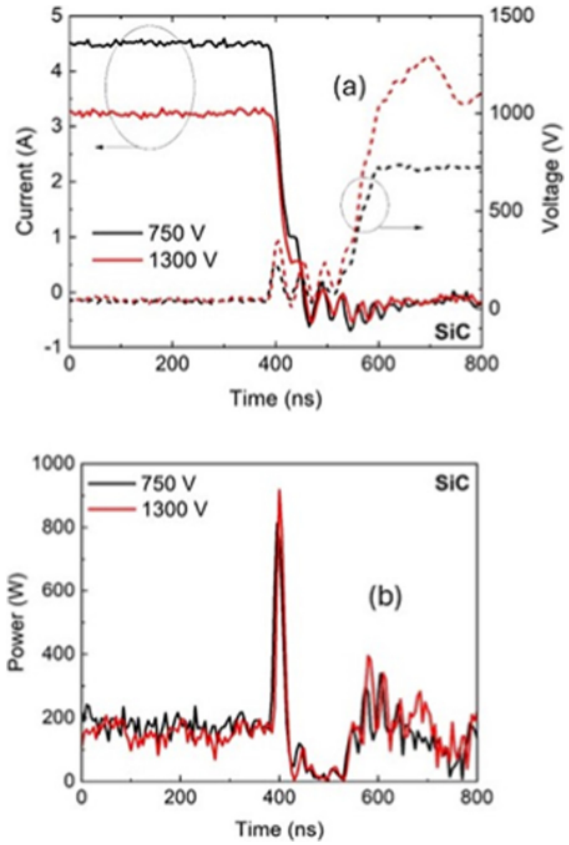

FIG. 7. Current (a) and power dissipation (b) switching waveforms for commercial SiC rectifiers when switching from either 750 or 1300 V.

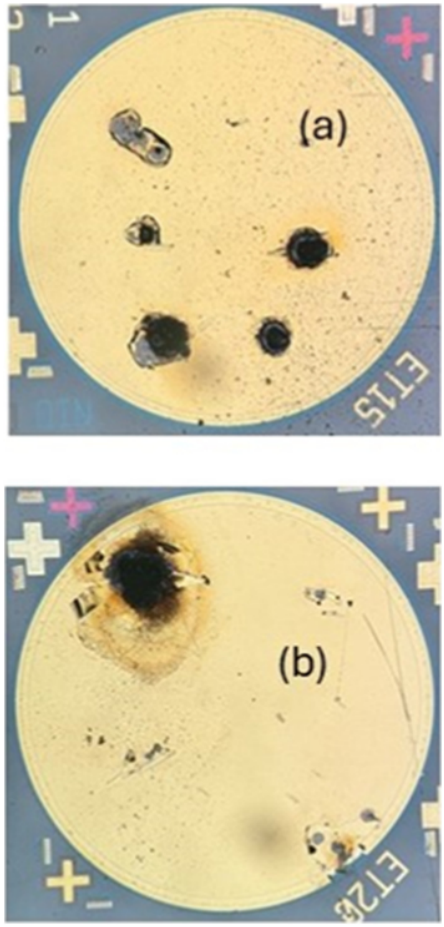

FIG. 8. Optical images of Ga_2O_3 rectifiers after breakdown (a) high current measurement with six probes at 4 A (b) after switching at 1500 V with 1% duty cycle.

DC-link voltages up to 500 V, currents up to 40 A, and peak voltage slew rates exceeding 100 V/ns. The performance of 600 μm thick TO247 packaged diodes with three different chip sizes was compared to commercial Si and SiC diodes of similar chip sizes.[12] Additionally, 200 μm thin Ga_2O_3 diodes with two different chip sizes were assembled in custom packages and compared to a commercial SiC diode of similar anode size.[37] The Ga_2O_3 diodes demonstrated switching properties comparable to SiC diodes. Under heavy load conditions, the buck converter efficiencies with Ga_2O_3 diodes surpassed those with a Si fast-recovery diode, though they remained lower than with SiC diodes. Future applications will require improvements in the trade-off between on-resistance and capacitive charge.[38]

A study by Jahdi *et al.*[50] assessed the performance of β-Ga_2O_3 rectifiers in the context of heavy-duty modular multilevel converter (MMC)-based voltage source converters and compared them with incumbent Si-IGBTs and SiC-FETs for high-voltage direct current (HVDC) and medium voltage direct current (MVDC) converter station applications. Various potential applications for β-Ga_2O_3 devices were considered, with MMC-VSC chosen for detailed examination due to its wide industry adoption and significant potential to leverage the high-voltage and high-efficiency operation of β-Ga_2O_3 devices.[50] The study demonstrates that NiO/Ga_2O_3 rectifiers when integrated with diamond can significantly enhance the performance of both MVDC and HVDC power converters in grid-level applications, with notable efficiency gains. This approach resulted in significantly lower thermal resistance, thereby reducing power dissipation.[50] This is important since the analysis by Hendricks *et al.*[37] showed that thermal limitations that degrade V_{ON} in Ga_2O_3 reduce the advantage of these rectifiers relative to SiC and GaN. Advanced thermal management solutions or soft-switched converter topologies will be essential to harness the efficiency advantages of β-Ga_2O_3 rectifiers. These advancements are necessary to facilitate the replacement of existing technologies across a wide range of applications.

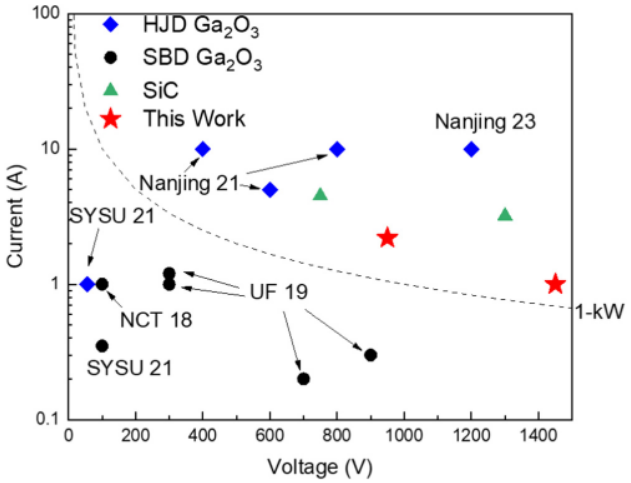

FIG. 9. Benchmark of reverse voltage vs forward current for vertical Ga_2O_3 rectifiers in the literature.

IV. SUMMARY AND CONCLUSIONS

NiO/β-Ga_2O_3 vertical heterojunction rectifiers with an absolute forward current of ~4 A and a breakdown voltage of 6.1 kV have been demonstrated on large-area devices (7.85×10^{-3} cm^2) with 15 μm thick drift layers. These devices switched from 1 A to −1450 V with a reverse recovery time (t_{rr}) of 75 ns, showing no significant dependence on voltage or current within the tested ranges. Even though the packaged SiC rectifiers cannot be directly compared to the Ga_2O_3 results, these measurements remain valuable for assessing the utility of Ga_2O_3.

These findings highlight the potential of p-n heterojunction NiO/Ga_2O_3 vertical Schottky rectifiers for high-power and high-speed switching applications, particularly considering recent reports indicating breakdown voltages up to 13.5 kV in similar structures.[26]

ACKNOWLEDGMENTS

The work at UF was performed as part of Interaction of Ionizing Radiation with Matter University Research Alliance (IIRM-URA), sponsored by the Department of the Defense, Defense Threat Reduction Agency under Award No. HDTRA1-20-2-0002. The content of the information does not necessarily reflect the position or the policy of the federal government, and no official endorsement should be inferred. The authors at National Yang Ming ChiaoTung University would like to acknowledge the National Science and Technology Council, Taiwan, for their financial support under Grant Nos. NSTC 112-2628-E-A49-015, MOST 107-2918-I-009-010, and 111-2628-E-A49-013.

AUTHOR DECLARATIONS

Conflict of Interest

The authors have no conflicts to disclose.

Author Contributions

Jian-Sian Li: Conceptualization (equal); Data curation (equal); Formal analysis (equal); Investigation (equal); Methodology (equal); Writing – original draft (equal). **Chao-Ching Chiang:** Conceptualization (equal); Data curation (equal); Formal analysis (equal); Investigation (equal); Methodology (equal); Writing – original draft (equal). **Hsiao-Hsuan Wan:** Conceptualization (equal); Data curation (equal); Formal analysis (equal); Investigation (equal); Methodology (equal); Writing – original draft (equal). **Meng-Hsun Yu:** Conceptualization (equal); Data curation (equal); Formal analysis (equal); Investigation (equal); Methodology (equal); Writing – original draft (equal). **Yi-Ting Lin:** Conceptualization (equal); Data curation (equal); Formal analysis (equal); Investigation (equal); Methodology (equal); Writing – original draft (equal). **Ying-Yu Yang:** Conceptualization (equal); Data curation (equal); Formal analysis (equal); Investigation (equal); Methodology (equal); Writing – original draft (equal). **Fan Ren:** Conceptualization (equal); Formal analysis (equal); Funding acquisition (equal); Investigation (equal); Methodology (equal); Project administration (equal); Writing – original draft (equal). **Yu-Te Liao:** Conceptualization (equal); Data curation (equal); Formal analysis (equal); Funding acquisition (equal); Investigation (equal); Methodology (equal); Project administration (equal); Writing – original draft (equal). **Stephen J. Pearton:** Conceptualization (equal); Data curation (equal); Funding acquisition (equal); Investigation (equal); Supervision (equal); Writing – original draft (equal).

DATA AVAILABILITY

The data that support the findings of this study are available within the article.

REFERENCES

[1]Mingfei Xu, Dawei Wang, Kai Fu, Dinusha Herath Mudiyanselage, Houqiang Fu, and Yuji Zhao, Oxford Open Mater. Sci. **2**, itac004 (2022).
[2]Kelly Woo, Zhengliang Bian, Maliha Noshin, Rafael Perez Martinez, Mohamadali Malakoutian, Bhawani Shankar, and Srabanti Chowdhury, J. Phys. Mater. **7**, 022003 (2024).
[3]S. J. Pearton, Jiancheng Yang, Patrick H. Cary, F. Ren, Jihyun Kim, Marko J. Tadjer, and Michael A. Mastro, Appl. Phys. Rev. **5**, 011301 (2018).
[4]Y. He, F. Zhao, B. Huang, T. Zhang, and H. Zhu, Materials **17**, 1870 (2024).
[5]Jincheng Zhang *et al.*, Nat. Commun. **13**, 3900 (2022).
[6]F. Zhou *et al.*, Nat. Commun. **14**, 4459 (2023).
[7]T. Oishi, K. Urata, M. Hashikawa, K. Ajiro, and T. Oshima, IEEE Electron Device Lett. **40**, 1393 (2019).
[8]J. Chen, X. Du, Q. Luo, X. Zhang, P. Sun, and L. Zhou, IEEE Trans. Power Electron. **35**, 13182 (2020).
[9]Y. Qin, B. Albano, J. Spencer, J. S. Lundh, B. Wang, C. Buttay, M. Tadjer, C. DiMarino, and Y. Zhang, J. Phys. D: Appl. Phys. **56**, 093001 (2023).
[10]Zhe Cheng, Samuel Graham, Hiroshi Amano, and David G. Cahill, Appl. Phys. Lett. **120**, 030501 (2022).
[11]F. Wilhelmi, S. Kunori, K. Sasaki, A. Kuramata, Y. Komatsu, and A. Lindemann, IEEE Trans. Power Electron. **37**, 3737 (2022).
[12]Florian Wilhelmi, Yuji Komatsu, Shinya Yamaguchi, Yuki Uchida, Tadashi Kase, Shinji Kunori, and Andreas Lindemann, IEEE Trans. Power Electron. **38**, 8406 (2023).
[13]Andrew J. Green *et al.*, APL Mater. **10**, 029201 (2022).

[14]A. K. Morya, Matthew C. Gardner, Bahareh Anvari, Liming Liu, Alejandro G. Yepes, Jesús Doval-Gandoy, and Hamid A. Toliyat, IEEE Trans. Transp. Electrif. **5**, 3 (2019).
[15]James Morra, Electron. Des. May 14, (2024), see https://www.electronicdesign.com/technologies/power/article/55039705/electronic-design-inside-a-hybrid-inverter-that-integrates-sic-mosfets-and-igbts.
[16]W. Li, K. Nomoto, Z. Hu, D. Jena, and H. G. Xing, IEEE Trans. Electron Devices **67**, 3938 (2020).
[17]Saurav Roy, Arkka Bhattacharyya, Carl Peterson, and Sriram Krishnamoorthy, Appl. Phys. Lett. **122**, 152101 (2023).
[18]Y. Kokubun, S. Kubo, and S. Nakagomi, Appl. Phys. Express **9**, 091101 (2016).
[19]Xing Lu, Yuxin Deng, Yanli Pei, Zimin Chen, and Gang Wang, J. Semicond. **44**, 061802 (2023).
[20]C. Liao *et al.*, IEEE Trans. Electron Devices **69**, 5722 (2022).
[21]P. Dong, J. Zhang, Q. Yan, Z. Liu, P. Ma, H. Zhou, and Y. Hao, IEEE Electron Device Lett. **43**, 765 (2022).
[22]Hang Dong *et al.*, IEEE Electron Device Lett. **40**, 1385 (2019).
[23]F. Zhou *et al.*, IEEE Trans. Power Electron. **37**, 1223 (2022).
[24]Jian-Sian Li, Chao-Ching Chiang, Xinyi Xia, Hsiao-Hsuan Wan, Fan Ren, and S. J. Pearton, J. Vac. Sci. Technol. A **41**, 043404 (2023).
[25]F. Wu *et al.*, IEEE Trans. Electron Devices **70**, 1199 (2023).
[26]Jian-Sian Li, Hsiao-Hsuan Wan, Chao-Ching Chiang, Timothy Jinsoo Yoo, Meng-Hsun Yu, Fan Ren, Honggyu Kim, Yu-Te Lia, and Stephen J. Pearton, ECS J. Solid State Sci. Technol. **13**, 035003 (2024).
[27]Jian-Sian Li, Chao-Ching Chiang, Xinyi Xia, Hsiao-Hsuan Wan, Fan Ren, and S. J. Pearton, J. Mater. Chem. C **11**, 7750 (2023).
[28]Jian-Sian Li, Xinyi Xia, Chao-Ching Chiang, David C. Hays, Brent P. Gila, Valentin Craciun, Fan Ren, and S. J. Pearton, J. Vac. Sci. Technol. A **41**, 013405 (2023).
[29]Jiancheng Yang, Chaker Fares, Randy Elhassani, Minghan Xian, Fan Ren, S. J. Pearton, Marko Tadjer, and Akito Kuramata, ECS J. Solid State Sci. Technol. **8**, Q3159 (2019).
[30]O. Slobodyan, J. Flicker, J. Dickerson, Jonah Shoemaker, Andrew Binder, Trevor Smith, Stephen Goodnick, Robert Kaplar, and Mark Hollis, J. Mater. Res. **37**, 849 (2022).
[31]Z. P. Wang *et al.*, Appl. Phys. Rev. **11**, 021413 (2024).
[32]Qinglong Yan, Hehe Gong, Jincheng Zhang, Jiandong Ye, Hong Zhou, Zhihong Liu, and Shengrui Xu, Appl. Phys. Lett. **118**, 044130 (2021).
[33]Y. H. Hong *et al.*, Appl. Phys. Lett. **12**, 128736 (2022).
[34]Y. Lv *et al.*, IEEE Trans. Power Electron. **36**, 6179 (2021).
[35]Q. He, W. Hao, Q. Li, Z. Han, S. He, Q. Liu, X. Zhou, G. Xu, and S. Long, Chin. Phys. B **32**, 128507 (2023).
[36]Advait Gilankar, Ahmad Ehteshamul Islam, Martha R. McCartney, Abishek Katta, Nabasindhu Das, David J. Smith, and Nidhin Kurian Kalarickal, Appl. Phys. Express **17**, 046501 (2024).
[37]N. S. Hendricks, J. J. Piel, A. E. Islam, and A. J. Green, "Analytical determination of unipolar diode losses in power switching and perspective for ultra-wide bandgap semiconductors," in *2024 IEEE Applied Power Electronics Conference and Exposition (APEC)*, Long Beach, CA, February 2024 (IEEE, New York, 2024), pp. 2670–2677.
[38]Franklin Lowa and Lowe Nouketcha, "On-resistance versus breakdown voltage capabilities of emerging semiconductors for opto- and power electronics," Ph.D. dissertation (University of Maryland, 2022).
[39]J. Yang, Fan Ren, Yen-Ting Chen, Yu-Te Liao, Chin-Wei Chang, Jenshan Lin, Marko J. Tadjer, S. J. Pearton, and Akito Kuramata, IEEE J. Electron Devices Soc. **7**, 57 (2019).
[40]J. Yang *et al.*, ECS J. Solid State Sci. Technol. **8**, Q3028 (2019).
[41]X. Lu, Xu Zhang, Huaxing Jiang, Xinbo Zou, Kei May Lau, and Gang Wang, Phys. Status Solidi A **217**, 190049 (2020).
[42]Jian-Sian Li, Chao-Ching Chiang, Xinyi Xia, Hsiao-Hsuan Wan, Fan Ren, and S. J. Pearton, ECS J. Solid State Sci. Technol. **12**, 085001 (2023).
[43]Jian-Sian Li, Chao-Ching Chiang, Xinyi Xia, Cheng-Tse Tsai, Fan Ren, Yu-Te Liao, and S. J. Pearton, ECS J. Solid State Sci. Technol. **11**, 105003 (2022).
[44]Y. Wei, Xiaorong Luo, Yuangang Wang, Juan Lu, Zhuolin Jiang, Jie Wei, Yuanjie Lv, and Zhihong Feng, IEEE Trans. Power Electron. **36**, 10976 (2021).
[45]F. Zhou *et al.*, Appl. Phys. Lett **119**, 262103 (2021).
[46]H. Gong *et al.*, IEEE Trans. Power Electron. **36**, 12213 (2021).
[47]Florian Wilhelmi, Yuji Komatsu, Shinya Yamaguchi, Yuki Uchida, Tadashi Kase, Shinji Kunori, and Andreas Lindemann, IEEE Trans. Power Electron. **38**, 7107 (2023).
[48]H. Gong *et al.*, IEEE Electron Device Lett. (published online 2024).
[49]Yen-Ting Chen, Jiancheng Yang, Fan Ren, Chin-Wei Chang, Jenshan Lin, S. J. Pearton, Marko J. Tadjer, Akito Kuramata, and Yu-Te Liao, ECS J. Solid State Sci. Technol. **8**, Q3229 (2019).
[50]S. Jahdi, A. S. Kumar, M. Deakin, P. C. Taylor, and M. Kuball, IEEE Open J. Power Electron. **5**, 554 (2024).